ACS OMEGA

Open Access



http://pubs.acs.org/journal/acsodf

Article

# Magnetism Induced by Azanide and Ammonia Adsorption in Defective Molybdenum Disulfide and Diselenide: A First-Principles Study

Guilherme S. L. Fabris, Bruno Ipaves, Raphael B. Oliveira, Humberto R. Gutierrez, Marcelo L. Pereira Junior,* and Douglas S. Galvão*

Cite This: *ACS Omega* 2026, 11, 6191−6197

Read Online

ACCESS | Metrics & More | Article Recommendations

**ABSTRACT:** Two-dimensional (2D) transition metal dichalcogenides (TMDs) have attracted considerable attention due to their tunable structural, electronic, and spin-related properties, particularly in the presence of point defects and molecular adsorbates. Motivated by these aspects, we have investigated using first-principles methods, the magnetic properties induced by azanide ($NH_2$) and ammonia ($NH_3$) adsorption on defective monolayers of molybdenum disulfide ($MoS_2$) and molybdenum diselenide ($MoSe_2$). Spin-polarized density functional theory (DFT) at the generalized gradient approximation (GGA) level, using the Perdew−Burke−Ernzerhof (PBE) functional, was employed to investigate the impact of mono- and divacancies on the local spin environment and the role of molecular adsorption in modifying magnetic behavior. The results show that pristine chalcogen vacancies do not generate magnetism, whereas the adsorption of $NH_2$ and $NH_3$ creates localized magnetic moments in Mo-based dichalcogenides. A notable case occurs for $MoSe_2$, where $NH_3$ dissociation into $NH_2$ and H fragments on the same side of the surface produces a net magnetic moment of 2.0 $\mu_B$. Tests performed on W-based dichalcogenides under equivalent conditions showed no magnetic response and are reported here only for comparison. These findings demonstrate that molecular adsorption combined with defect engineering can be a practical approach to tune magnetism in 2D materials, with potential relevance for spintronic and sensing applications.

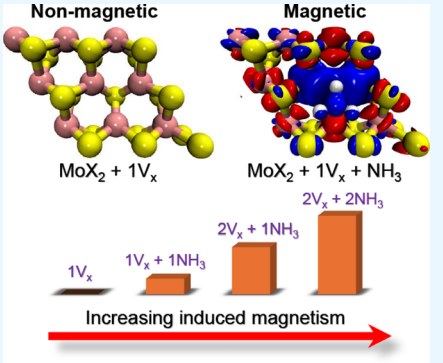


## INTRODUCTION

Two-dimensional (2D) transition metal dichalcogenides (TMDs) have attracted considerable attention due to their tunable electronic,[1,2] optical,[3,4] and structural[5,6] properties, which make them relevant for diverse technological applications.[6] Beyond their intrinsic characteristics, the behavior of TMD monolayers can be significantly modified by the presence of point defects, such as mono and divacancies, as well as by the adsorption of gas molecules.[7−11] Previous studies indicate that vacancies of chalcogen atoms (S or Se) typically do not induce spin density variations in Mo-based dichalcogenides. In contrast, metal vacancies can give rise to localized magnetic moments.[12−14]

The role of molecular adsorption in defective TMDs has been examined for species such as $H_2O$, $O_2$, and $O_3$, which can stabilize near vacancy sites and, in some cases, dissociate to alter the local electronic structure.[8,15] In parallel, defects such as vacancies and interstitials, which are inevitably formed during material growth, may generate local magnetic moments capable of interacting over long ranges.[13] These findings underline the importance of modifications in the spin density environment and suggest that the impact of adsorbates depends strongly on the type of vacancy and the surrounding chemical environment.

While several studies have examined adsorption[16,17] and defect[18,19] effects in TMDs, systematic investigations specifically addressing small adsorbates such as $NH_2$ and $NH_3$ on Mo-based TMDs remain underexplored. Moreover, the combined influence of mono- and divacancies together with multiple adsorbates, and its impact on the spatial distribution of local magnetic moments, has not been comprehensively explored. Addressing this knowledge gap is important for understanding spin distributions in 2D TMDs and for advancing the design of sensor and spintronic applications.[20,21]

In this work, we have carried out first-principles density functional theory (DFT) simulations to investigate the effects

Received: October 20, 2025
Revised: January 9, 2026
Accepted: January 14, 2026
Published: January 20, 2026

of azanide ($NH_2$) and ammonia ($NH_3$) adsorption on monolayers of $MoS_2$ and $MoSe_2$ containing mono- and divacancies. We analyzed how adsorbates modify the local spin densities and identified conditions under which magnetism can be induced in otherwise nonmagnetic defective chalcogens. For comparison, additional tests on $WS_2$ and $WSe_2$ showed no magnetic response under equivalent conditions. These results provide insights into adsorbate-driven spin distortions in Mo-based dichalcogenides and contribute to a better understanding of defect-engineered 2D materials with tunable spin properties.

## METHODOLOGY

To investigate the structural, electronic, and spin densities of $MoX_2$ (X = S or Se) with mono and divacancies, as well as the effect of ammonia and azanide molecules on their magnetic properties, we performed ab initio simulations based on DFT[22] as implemented in the SIESTA code.[23,24] The exchange-correlation effects were described using the PBE (Perdew−Burke−Ernzerhof) functional,[25] combined with a DZP (double-$\zeta$ polarization) basis set composed of numerical atomic orbitals. This choice follows the widespread use of PBE in studies of defect states and adsorption effects in Mo-based TMDs.[12,15,26,27] A real-space mesh cutoff of 400 Ry and a Γ-centered Monkhorst−Pack grid[28] of 8 × 8 × 1 and 4 × 4 × 1 $k$-points were adopted for the monolayer unit cell and the 3 × 3 × 1 supercell, respectively. A vacuum region of 25 Å was included along the perpendicular direction to avoid spurious interactions between periodic images. The 3 × 3 × 1 supercell provides defect-image separations larger than 9 Å for $MoS_2$ and $MoSe_2$, ensuring a reliable description of isolated vacancies and of the $NH_2/NH_3$ adsorption configurations considered. The convergence threshold for the self-consistent field cycle was set to $10^{-4}$ for the density matrix tolerance, and the structural relaxation was performed until the residual forces were smaller than 0.05 eV/Å. All calculations were carried out within a spin-polarized framework. The nanostructures and the spin density were visualized using the Visual Molecular Dynamics (VMD) software,[29] and an isovalue of 0.001 was adopted for the spin-density plots.

## RESULTS

Initially, we investigated the changes in the spin densities of $MoS_2$ and $MoSe_2$ monolayers in the presence of defects. As a first step, we optimized the pristine $MoX_2$ structures to validate the accuracy of the computational setup. The optimized lattice parameters were $a = b = 3.17$ Å for $MoS_2$ and $a = b = 3.31$ Å for $MoSe_2$, with corresponding Mo−S and Mo−Se bond lengths of 2.42 and 2.54 Å. The calculated electronic band gaps of pristine $MoS_2$ and $MoSe_2$ are 1.14 and 1.08 eV, respectively. These values are consistent with previous theoretical reports,[7,8,26,27] as expected given the well-known tendency of PBE-based calculations to underestimate band gaps. The results are summarized in Table 1, confirming the reliability of the adopted methodology.

After validating the computational parameters, we created a 3 × 3 × 1 supercell of $MoX_2$ (X = S or Se) and introduced mono- and divacancy models. The divacancy was considered in two configurations: both vacancies on the same side of the monolayer and one vacancy on each side of the supercell (alternated), as illustrated in Figure 1. These defective models were then used to investigate the influence of $NH_3$ adsorption at the vacancy sites, with representative configurations shown in Figure 1.

**Table 1. Comparison of the In-plane Lattice Constant $a$ (Å) and Electronic Band Gap $E_g$ (eV) of Monolayer $MoX_2$ Obtained in This Work, Together With Representative Hybrid-functional and Experimental Values**

| | $a$ (Å) | | | $E_g$ (eV) | | |
|---|---|---|---|---|---|---|
| material | this work | hybrid[30] | expt.[31,32] | this work | hybrid[30] | expt.[31,32] |
| $MoS_2$ | 3.17 | 3.23 | 3.16 | 1.14 | 1.56 | 1.80 |
| $MoSe_2$ | 3.31 | 3.38 | 3.30 | 1.08 | 1.38 | 1.54−1.57 |

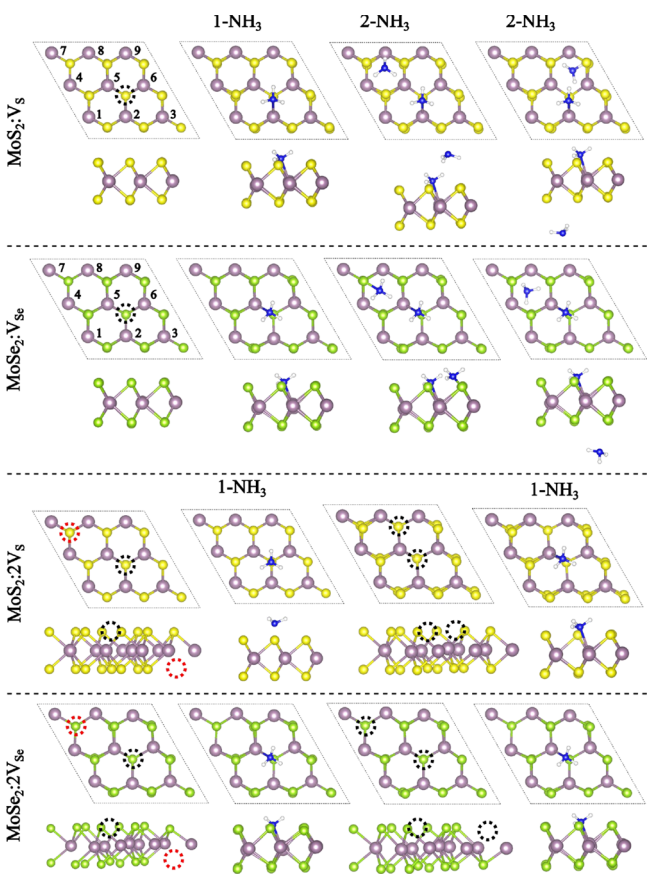


**Figure 1.** Schematic illustration of the top and side views of a 3 × 3 × 1 supercell of $MoX_2$ (X = S or Se) featuring one vacancy (VX) and two vacancies (2VX). The figure includes cases investigated with the adsorption of one $NH_3$ molecule and two $NH_3$ molecules. Dashed black and red circles indicate the vacancy positions, while the numbers 1−9 correspond to the label of the Mo atoms referenced in all tables.

Before analyzing the adsorption results, it is important to note that the dangling bonds associated with chalcogen vacancies are explicitly present in our defective $MoX_2$ models. Removing an S or Se atom leaves the surrounding Mo atoms unsaturated, generating localized states at the vacancy site; these vacancy-induced dangling bonds interact directly with the adsorbed $NH_2/NH_3$ species and play an essential role in the magnetic behavior discussed below. All structures discussed in this work were fully relaxed before evaluating their magnetic properties, and the analysis focuses on the response associated with $NH_2$ and $NH_3$ molecules near





https://doi.org/10.1021/acsomega.5c10979
ACS Omega 2026, 11, 6191−6197

vacancy sites. The adsorption of azanide or ammonia on $MoX_2$ generally occurs via physisorption, which may lead to slight variations in the electronic band gap value due to polarization effects. However, they do not introduce midgap states.[33]

The creation of S and Se vacancies resulted in defective structures without spin density variations, in agreement with previous reports that describe the absence of magnetism in such systems.[7,8,26,27] The adsorption of $H_2O$ and $NH_3$ in Mo-based TMDs has been examined in the literature, and most studies indicate negligible changes in the spin environment.[8,9,34] Nevertheless, the dissociation of $H_2O$ at vacancy sites has been reported to induce significant modifications in the local spin distribution.[8,15]

For the $NH_3$ adsorption, a single molecule stabilizes near the vacancy site at distances of 2.38 and 2.36 Å from the nearest Mo atom in $MoS_2$ and $MoSe_2$, respectively. When two $NH_3$ molecules are present, one occupies a position similar to that in the single-molecule case. At the same time, the second stabilizes further from the surface, with distances to the nearest S or Se atoms ranging from 1.79 to 2.94 Å.

A key result of this study is that $NH_3$ adsorption increases the local magnetic moment of Mo atoms near vacancy sites in both $MoS_2$ and $MoSe_2$ (Figures 2 and 3, Tables 2 and 3). This

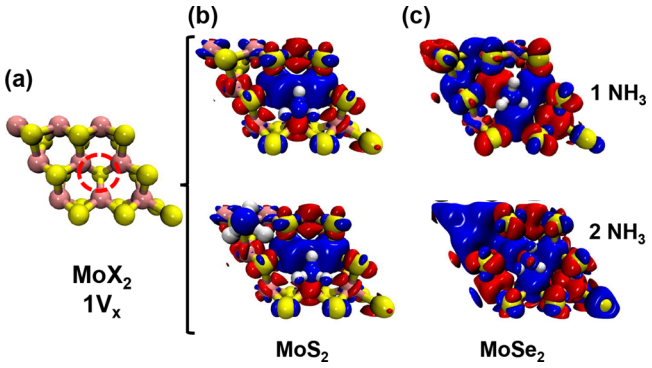


**Figure 2.** Spin density maps for (a) $MoX_2$ monolayers with a monovacancy, (b) $MoS_2$, and (c) $MoSe_2$ with one and two adsorbed $NH_3$ molecules. The dashed red circle indicates the position of the vacancy. In the maps, red color indicates spin-up density, while blue represents spin-down density.

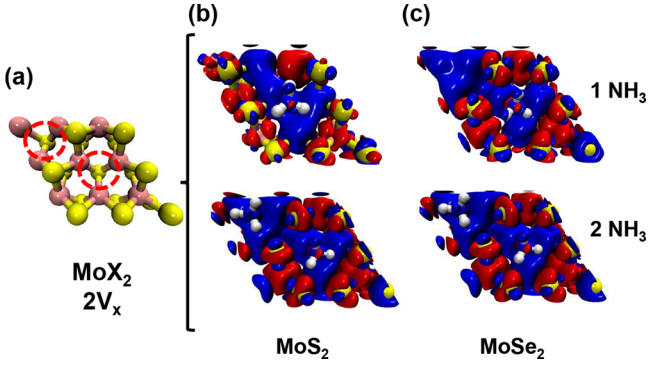


**Figure 3.** Spin density maps for (a) $MoX_2$ monolayers with a divacancy, (b) $MoS_2$, and (c) $MoSe_2$ with one and two adsorbed $NH_3$ molecules. The dashed red circle indicates the position of the vacancy. In the maps, red color indicates spin-up density, while blue represents spin-down density.

effect, rarely reported in the literature, was observed at specific Mo atoms surrounding the adsorption site. In the case of a divacancy on the same side of the monolayer, the increase became more pronounced, with additional Mo atoms developing nonzero magnetic moments. Quantitatively, $MoS_2$ exhibited an enhancement of approximately 21.3%, while $MoSe_2$ showed a much larger increase of 200%. By contrast, the alternated divacancy configuration did not modify the response, yielding values comparable to those of the single-vacancy case. These results indicate that exposure to $NH_3$ can enhance induced magnetism in Mo-based dichalcogenides, as illustrated by the spin density difference maps in Figures 2 and 3.

We further investigated the resulting magnetic moment behavior induced by the adsorption of two $NH_3$ molecules on $MoS_2$ and $MoSe_2$ surfaces with a single vacancy. For both $MoS_2$ and $MoSe_2$, placing two $NH_3$ molecules on the same side of the surface resulted in a nonzero magnetic moment, which was also observed when positioning one $NH_3$ molecule on each side of the surface. In the case of $MoS_2$, the magnetic moment behavior was similar to that observed in config-

**Table 2. Spin-Polarized Electron Distribution for Mo Atoms Near Vacancy Sites with One $NH_3$ Adsorption in $MoS_2$ and $MoSe_2$[a]**

| | $MoS_2$ | | $MoSe_2$ | |
|---|---|---|---|---|
| Mo atom no | $\mu_{Local}$ (1 $V_S$) | $\mu_{Local}$ (2 $V_S$) | $\mu_{Local}$ (1 $V_{Se}$) | $\mu_{Local}$ (2 $V_{Se}$) |
| 1 | −0.058 | −0.133 | 0.065 | −0.984 |
| 2 | −0.222 | 1.158 | 2.098 | 1.265 |
| 3 | −0.058 | −0.232 | −1.079 | −0.758 |
| 4 | −0.104 | −0.265 | 0.472 | 2.196 |
| 5 | 1.418 | 1.287 | −1.474 | 1.410 |
| 6 | 1.417 | 1.049 | 2.098 | 1.265 |
| 7 | 0.026 | −0.075 | −0.433 | 1.303 |
| 8 | 0.025 | 1.067 | 0.472 | 2.196 |
| 9 | −0.332 | −1.150 | 0.065 | −0.984 |

[a]The table presents the local magnetic moments ($\mu_{Local}$) in units of $\mu_B$ at each Mo atom (labeled according to Figure 1), calculated as the difference in spin-up and spin-down electron populations. Notably, Mo atoms at specific positions exhibit non-zero resulting magnetic moments, with $\mu_{Local}$ values possibly indicating magnetic response. This effect intensifies with divacancy configurations, as indicated by the increased magnetic moments on other Mo atoms.

**Table 3. Spin-Polarized Electron Distribution for Mo Atoms Near Vacancy Sites with Two $NH_3$ Adsorptions in $MoS_2$ and $MoSe_2$ in Different Positions[a]**

| | $MoS_2$ | | $MoSe_2$ | |
|---|---|---|---|---|
| Mo atom no | $\mu_{Local}$ (same side) | $\mu_{Local}$ (opposite side) | $\mu_{Local}$ (same side) | $\mu_{Local}$ (opposite side) |
| 1 | −0.058 | −0.058 | −0.369 | 0.070 |
| 2 | −0.226 | −0.227 | 1.933 | 2.101 |
| 3 | −0.060 | −0.058 | −0.612 | −1.089 |
| 4 | −0.102 | −0.104 | −0.697 | 0.447 |
| 5 | 1.424 | 1.415 | 1.655 | −1.481 |
| 6 | 1.422 | 1.410 | 1.925 | 2.104 |
| 7 | 0.024 | 0.031 | −0.681 | −0.409 |
| 8 | 0.027 | 0.032 | −0.440 | 0.463 |
| 9 | −0.340 | −0.330 | −0.503 | 0.049 |

[a]The table presents the Mo local magnetic moments ($\mu_{Local}$) in $\mu_B$, illustrating the resulting magnetic moment response (atom numbers labeled according to Figure 1). When the molecules were positioned on opposite sides for $MoSe_2$, the $\mu_{Local}$ values resemble those from the single vacancy and one $NH_3$ case (see Table 2).





https://doi.org/10.1021/acsomega.5c10979
ACS Omega 2026, 11, 6191−6197

urations with a single vacancy and one $NH_3$ molecule. Similarly, for $MoSe_2$, placing one $NH_3$ on each side of the surface produced a nonmagnetic moment response comparable to that observed in configurations with a single vacancy and one $NH_3$ (see Tables 2 and 3).

We have extended our investigation to the adsorption of $NH_2$ molecules on $MoS_2$ and $MoSe_2$ surfaces with mono and divacancies. The results, presented in Figure 4, Tables 4 and 5,

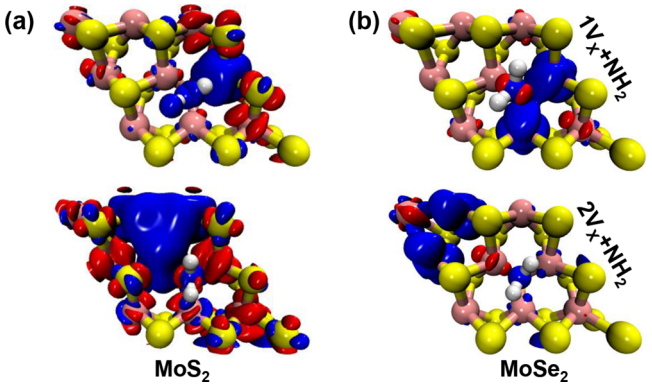


**Figure 4.** Spin density maps for (a) $MoS_2$ and (b) $MoSe_2$ monolayers with one and two vacancies (top and bottom figures, respectively), and with one adsorbed $NH_2$ molecule.

**Table 4. Spin-Polarized Electron Distribution for Mo Atoms Near Vacancy Sites with One $NH_2$ Adsorption in $MoS_2$ and $MoSe_2$[a]**

| | $MoS_2$ | | $MoSe_2$ | |
|---|---|---|---|---|
| Mo atom no | $\mu_{Local}$ (vacancy) | $\mu_{Local}$ (divacancy) | $\mu_{Local}$ (vacancy) | $\mu_{Local}$ (divacancy) |
| 1 | 0.056 | −0.032 | 0.000 | 0.002 |
| 2 | 0.032 | 0.692 | 0.041 | 0.020 |
| 3 | −0.045 | −0.051 | −0.028 | −0.008 |
| 4 | −0.026 | 0.008 | 0.007 | 0.482 |
| 5 | 0.032 | 0.012 | 0.036 | −0.050 |
| 6 | 0.911 | 0.056 | 0.934 | 0.023 |
| 7 | −0.026 | −0.010 | 0.009 | −0.033 |
| 8 | 0.049 | 0.095 | 0.003 | 0.508 |
| 9 | −0.044 | 0.188 | −0.026 | 0.002 |

[a]The table presents the local magnetic moments ($\mu_{Local}$) in $\mu_B$ at each Mo atom (labeled according to Figure 1), calculated by the difference in spin-up and spin-down electron populations. Notably, Mo atoms at specific positions exhibit induced magnetic moments, with $\mu_{Local}$ values highlighting the magnetic moment response. Unlike the $NH_3$ case, this effect does not increase with divacancy configurations.

reveal distinct magnetic moment behaviors compared to the $NH_3$ case, providing further insights into the role of adsorbates and vacancy configurations in spin density variations.

For $NH_2$ adsorption, we observed a magnetic response in Mo atoms near the vacancy sites for both $MoS_2$ and $MoSe_2$. From the simulations, it is evident that the magnetic moment in $MoS_2$ increases substantially when a divacancy is introduced; however, this behavior was not observed in $MoSe_2$. In $MoS_2$, significant magnetic moments appeared at specific Mo atoms, with local magnetic moments ($\mu_{Local}$) reaching up to 0.911 $\mu_B$ for the single vacancy, and showing only slight variations under divacancy conditions. Conversely, in $MoSe_2$, the magnetic moments were generally weaker, with values below 0.5 $\mu_B$ in most cases (Table 4).

**Table 5. Spin-Polarized Electron Distribution for Mo Atoms Near Vacancy Sites with Two $NH_2$ Adsorptions in $MoS_2$ and $MoSe_2$[a]**

| | $MoS_2$ | | $MoSe_2$ | |
|---|---|---|---|---|
| Mo atom no | $\mu_{Local}$ (same side) | $\mu_{Local}$ (opposite side) | $\mu_{Local}$ (same side) | $\mu_{Local}$ (opposite side) |
| 1 | 0.048 | 0.022 | 0.000 | 0.197 |
| 2 | 0.029 | 0.040 | 0.000 | 0.029 |
| 3 | −0.045 | −0.022 | 0.000 | −0.036 |
| 4 | −0.029 | 0.006 | 0.000 | −0.008 |
| 5 | 0.030 | 0.043 | 0.000 | 0.008 |
| 6 | 0.910 | 0.825 | 0.000 | 0.973 |
| 7 | −0.022 | −0.007 | 0.000 | 0.032 |
| 8 | 0.040 | 0.011 | 0.000 | −0.002 |
| 9 | −0.043 | −0.024 | 0.000 | 0.007 |

[a]The table presents the Mo local magnetic moments ($\mu_{Local}$) in $\mu_B$, illustrating the magnetic response (atom numbers labeled according to Figure 1). We found no magnetism in $MoSe_2$ for the configuration with both $NH_2$ molecules on the same side.

These findings suggest that $NH_2$ adsorption alone is sufficient to induce an increase in the resulting magnetic moment of Mo atoms, but that the effect does not scale with increasing vacancy density, as observed in the $NH_3$ case. This suggests that $NH_2$ molecules interact differently with the $MoX_2$ surface, possibly due to their smaller size and distinct electronic configuration compared to $NH_3$, resulting in distinct bonding characteristics and charge redistribution near the vacancy sites. The absence of a significant enhancement in the total magnetic moment for divacancy configurations further emphasizes the localized nature of the magnetic response induced by $NH_2$.

Following this, we further investigated the magnetic moment behavior induced by two $NH_2$ molecules adsorbed on $MoS_2$ and $MoSe_2$ surfaces with a single vacancy. For $MoS_2$, adsorbing two $NH_2$ molecules on the surface resulted in local magnetic moments distributed among Mo atoms near the vacancy site (Table 5). For $MoSe_2$, positioning one $NH_2$ molecule on each side of the surface induced a magnetic moment; however, placing two $NH_2$ molecules on the same side of the surface resulted in a zero magnetic moment. For clarity, Tables 2−6 report the local magnetic moments of Mo atoms near the vacancy sites, whereas the total magnetic moment of each configuration is summarized in Figure 5.

We also investigated configurations in which $NH_2$ and H fragments are adsorbed on the surface, representing dissociated $NH_3$ species. We considered two distinct arrangements: both fragments located on the same side of the exposed surface, and an alternating configuration in which $NH_2$ and H are positioned on opposite sides (top and bottom). The corresponding results are reported in Table 6. For $MoS_2$, a net magnetic moment of 0.444 $\mu_B$ was observed in both configurations, indicating that the dissociation induces magnetization regardless of the spatial distribution of the fragments. In contrast, for $MoSe_2$, a net magnetic moment of 2.0 $\mu_B$ was only found when both $NH_2$ and H were adsorbed on the same side of the surface, while the alternating configuration did not result in any net magnetization.

These results suggest that the magnetic response of the system is highly sensitive to both the nature of the chalcogen atom and the spatial arrangement of the dissociated species. The stronger magnetization observed in $MoSe_2$ under specific





https://doi.org/10.1021/acsomega.5c10979
ACS Omega 2026, 11, 6191−6197

**Table 6. Spin-Polarized Electron Distribution for Mo Atoms Near Vacancy Sites with One $NH_2$ and One H Adsorption in $MoS_2$ and $MoSe_2$[a]**

| | $MoS_2$ | | $MoSe_2$ | |
|---|---|---|---|---|
| Mo atom no | $\mu_{Local}$ (same side) | $\mu_{Local}$ (opposite side) | $\mu_{Local}$ (same side) | $\mu_{Local}$ (opposite side) |
| 1 | −0.005 | 0.000 | 0.064 | 0.000 |
| 2 | −0.011 | −0.018 | 0.042 | 0.000 |
| 3 | −0.026 | −0.034 | 0.003 | 0.000 |
| 4 | −0.038 | −0.047 | 0.678 | 0.000 |
| 5 | −0.014 | −0.019 | 0.023 | 0.000 |
| 6 | 0.601 | 0.620 | 0.922 | 0.000 |
| 7 | −0.038 | −0.047 | 0.015 | 0.000 |
| 8 | −0.041 | −0.021 | −0.001 | 0.000 |
| 9 | −0.025 | −0.035 | −0.029 | 0.000 |

[a]The table presents the local magnetic moments ($\mu_{Local}$) in $\mu_B$ at each Mo atom (labeled according to Figure 1), calculated by the difference in spin-up and spin-down electron populations. Notably, Mo atoms at specific positions exhibit induced magnetic moments, with $\mu_{Local}$ values highlighting the magnetic moment response.

adsorption geometry may be attributed to enhanced spin polarization effects mediated by the heavier selenium atoms and the localized electronic interactions between coadsorbed fragments. This highlights the potential for tuning magnetic properties in 2D materials via controlled molecular dissociation and adsorption configurations.

We extended our investigation to W-based dichalcogenides, $WS_2$ and $WSe_2$, using the same approach used to $MoS_2$ and $MoSe_2$. Initially, we explored the magnetic moment behavior of the pristine monolayers as well as systems with mono and divacancies ($V_X$ and 2 $V_X$, respectively). Unlike $MoX_2$, no resulting magnetic moment was observed in $WS_2$ or $WSe_2$ for any vacancy configuration, with the magnetic moments consistently obtained as zero.

Additionally, we examined the adsorption of one and two $NH_3$ molecules on the vacancy sites of $WS_2$ and $WSe_2$. In all cases, the systems remained with a zero resulting magnetic moment, indicating that $NH_3$ adsorption does not induce spin density changes in these materials, even in the presence of vacancies. Nonzero spin density emerged only when a W atom was removed instead of an S or Se atom. This suggests that the absence of a resulting magnetic moment in the previous configurations arises from the electronic structure of the W atoms and their interaction with the surrounding lattice. This behavior is consistent with previous theoretical studies, which reported that magnetism appears only in the presence of $W_2$ or $WSe_6$ vacancies.[12]

Our results show that creating S or Se vacancies in $MoX_2$ does not inherently lead to a nonzero resulting magnetic moment; however, the presence of $NH_2$ or $NH_3$ molecules can modify the local environment, leading to a nonzero magnetic moment. This effect becomes more pronounced under conditions of high defect density and low $NH_3$ concentration. On the other hand, no resulting magnetic moment was observed in $WX_2$ systems with either mono- or divacancies of X. These findings highlight a significant contrast between the spin density properties of Mo- and W-based dichalcogenides under similar conditions, emphasizing the critical role of the transition metal in determining the resulting magnetic moment behavior of these materials. Finally, we note that the simultaneous presence of different vacancy types, such as chalcogen and metal vacancies, is expected to introduce additional localized states and may lead to distinct magnetic responses. A reliable treatment of such mixed-defect configurations would require significantly larger supercells to avoid artificial interactions, thereby substantially increasing the computational cost. These systems, therefore, represent an interesting direction for future investigations.

## CONCLUSIONS

In summary, spin-polarized DFT simulations were employed to investigate the effects of $NH_2$ and $NH_3$ adsorption on defective $MoX_2$ (X = S, Se) monolayers. The results confirm that pristine chalcogen vacancies do not induce magnetism, while molecular adsorption can create localized magnetic moments in Mo-based dichalcogenides. A notable case was observed for $MoSe_2$, where $NH_3$ dissociation into $NH_2$ and H fragments on the same side of the surface produced a net magnetic moment of 2.0 $\mu_B$. For comparison, W-based TMDs were also examined and remained nonmagnetic under equivalent conditions. These findings suggest that molecular adsorption, combined with defect engineering, influences the magnetic behavior of Mo-based TMDs, providing insights for

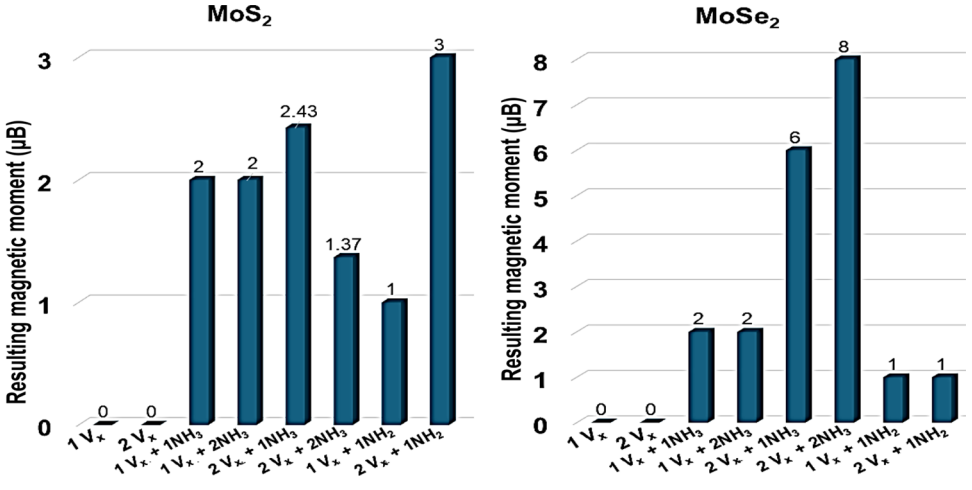


**Figure 5.** Resulting magnetic moment of each case considered in this work. The results reflect the values obtained from the same side vacancy and $NH_3$/$NH_2$ molecule adsorption.



https://doi.org/10.1021/acsomega.5c10979
ACS Omega 2026, 11, 6191−6197

future studies on spin-related phenomena in low-dimensional systems.

## AUTHOR INFORMATION


### Corresponding Authors

**Marcelo L. Pereira Junior** − *Department of Materials Science and NanoEngineering, Rice University, Houston, Texas 77005, United States; Department of Electrical Engineering, College of Technology, University of Brasília, Brasília, Federal District 70910-900, Brazil;* orcid.org/0000-0001-9058-510X; Email: marcelo.lopes@unb.br

**Douglas S. Galvão** − *Applied Physics Department and Center for Computational Engineering & Sciences, State University of Campinas, Campinas, São Paulo 13083-970, Brazil;* orcid.org/0000-0003-0145-8358; Email: galvao@ifi.unicamp.br

### Authors

**Guilherme S. L. Fabris** − *Applied Physics Department and Center for Computational Engineering & Sciences, State University of Campinas, Campinas, São Paulo 13083-970, Brazil;* orcid.org/0000-0002-0830-5787

**Bruno Ipaves** − *Applied Physics Department and Center for Computational Engineering & Sciences, State University of Campinas, Campinas, São Paulo 13083-970, Brazil;* orcid.org/0000-0003-2908-4589

**Raphael B. Oliveira** − *Department of Materials Science and NanoEngineering, Rice University, Houston, Texas 77005, United States;* orcid.org/0009-0008-3913-6614

**Humberto R. Gutierrez** − *Department of Physics, University of South Florida, Tampa, Florida 33620, United States;* orcid.org/0000-0001-8997-5274

Complete contact information is available at: https://pubs.acs.org/10.1021/acsomega.5c10979



### Funding

The Article Processing Charge for the publication of this research was funded by the Coordenacao de Aperfeicoamento de Pessoal de Nivel Superior (CAPES), Brazil (ROR identifier: 00x0ma614).

### Notes

The authors declare no competing financial interest.

## ACKNOWLEDGMENTS

R.B.O. thanks the National Council for Scientific and Technological Development (CNPq) process numbers 151043/2024-8 and 200257/2025-0. B.I. acknowledges support from CNPq and São Paulo Research Foundation (FAPESP) process numbers 153733/2024-1 and 2024/11016-0. G.S.L.F. acknowledges support from FAPESP process number #2024/03413-9. M.L.P.J. acknowledges financial support from FAPDF (grant 001 93-00001807/2023-16), CNPq (grants 444921/2024-9 and 308222/2025-3), and CAPES (grant 88887.005164/2024-00). D.S.G. acknowledges the Center for Computing in Engineering and Sciences at Unicamp forfinancial support through the FAPESP/CEPID Grant #2013/08293-7. The authors thank the Coaraci Supercomputer Center for computer time (Fapesp grant #2019/17874-0).


## REFERENCES


(1) Gusakova, J.; Wang, X.; Shiau, L. L.; Krivosheeva, A.; Shaposhnikov, V.; Borisenko, V.; Gusakov, V.; Tay, B. K. Electronic properties of bulk and monolayer TMDs: theoretical study within DFT framework (GVJ-2e method). *phys. status solidi (a)* **2017**, *214*, No. 1700218.

(2) Xia, J.; Yan, J.; Shen, Z. X. Transition metal dichalcogenides: structural, optical and electronic property tuning via thickness and stacking. *FlatChem.* **2017**, *4*, 1−19.

(3) Vu, T. V.; Lavrentyev, A.; Thuan, D. V.; Nguyen, C. V.; Khyzhun, O.; Gabrelian, B.; Tran, K. C.; Luong, H. L.; Tung, P. D.; Pham, K. D.; et al. Electronic properties and optical behaviors of bulk and monolayer ZrS2: A theoretical investigation. *Superlattices Microstruct.* **2019**, *125*, 205−213.

(4) Ermolaev, G. A.; Stebunov, Y. V.; Vyshnevyy, A. A.; Tatarkin, D. E.; Yakubovsky, D. I.; Novikov, S. M.; Baranov, D. G.; Shegai, T.; Nikitin, A. Y.; Arsenin, A. V.; et al. Broadband optical properties of monolayer and bulk MoS2. *npj 2D Mater. Appl.* **2020**, *4*, 21.

(5) Ipaves, B.; de Oliveira, R. B.; da Silva Lopes Fabris, G.; Batzill, M.; S. Galvão, D. Unraveling Mn intercalation and diffusion in NbSe2 bilayers through DFTB simulations. *Phys. E: Low Dimens. Syst. Nanostruct.* **2026**, *175*, No. 116355.

(6) Joseph, S.; Mohan, J.; Lakshmy, S.; Thomas, S.; Chakraborty, B.; Thomas, S.; Kalarikkal, N. A review of the synthesis, properties, and applications of 2D transition metal dichalcogenides and their heterostructures. *Mater. Chem. Phys.* **2023**, *297*, No. 127332.

(7) Haldar, S.; Vovusha, H.; Yadav, M. K.; Eriksson, O.; Sanyal, B. Systematic study of structural, electronic, and optical properties of atomic-scale defects in the two-dimensional transition metal dichalcogenides MX 2 (M= Mo, W; X= S, Se, Te). *Phys. Rev. B* **2015**, *92*, No. 235408.

(8) Devi, A.; Dhiman, N.; Kumar, N.; Alfalasi, W.; Kumar, A.; Ahluwalia, P.; Singh, A.; Tit, N. Ferromagnetism in defected TMD (MoX2, X= S, Se) monolayer and its sustainability under O2, O3, and H2O gas exposure: DFT study. *Nanomaterials* **2023**, *13*, 1642.

(9) De, S.; Rajbhar, M. K.; Sanyal, G.; Chakraborty, B.; Sharma, C. S.; Chatterjee, S. Augmented ammonia sensing of ion-beam modified MoSe2. *Surfaces and Interfaces* **2024**, *49*, No. 104394.

(10) Dang, D. T.-X.; Pham, Y. T.-H.; Zhou, D.; Le, D.-N.; Terrones, M.; Phan, M.-H.; Woods, L. M. Interface Magnetism in Vanadium-doped MoS2/Graphene Heterostructures. *RSC Appl. Interfaces* **2025**, *2*, 1650−1660.

(11) Sharma, R.; Dang, D. T.-X.; Woods, L. M. Magnetism at the interface of $MoSe_2/V_2O_5$ heterostructures. *J. Phys. Chem. Solids* **2025**, *211*, No. 113403.

(12) Yang, D.; Fan, X.; Zhang, F.; Hu, Y.; Luo, Z. Electronic and magnetic properties of defected monolayer WSe2 with vacancies. *Nanoscale Res. Lett.* **2019**, *14*, 192.

(13) Gaikwad, P. V.; Hoang, T. T.; Park, S.; Bang, J. Long-range magnetic interaction of native defects in transition metal dichalcogenides. *RSC Adv.* **2025**, *15*, 6585−6592.

(14) Oliveira, M. J.; Medeiros, P. V.; Sousa, J. R.; Nogueira, F.; Gueorguiev, G. K. Optical and magnetic excitations of metal-encapsulating Si cages: A systematic study by time-dependent density functional theory. *J. Phys. Chem. C* **2014**, *118*, 11377−11384.

(15) Ataca, C.; Ciraci, S. Dissociation of H 2 O at the vacancies of single-layer MoS 2. *Physical Review B—Condensed Matter and Materials. Physics* **2012**, *85*, No. 195410.

(16) Szary, M. J.; Radomski, P. Unveiling the chemical underpinnings behind the enhanced adsorption interaction of NO2 on MoS2, MoSe2, and MoTe2 transition metal dichalcogenides. *J. Phys. Chem. C* **2023**, *127*, 21374−21386.

(17) Lee, B. H.; Fatheema, J.; Akinwande, D.; Wang, W. Understanding and predicting trends in adsorption energetics on monolayer transition metal dichalcogenides. *npj 2D Mater. Appl.* **2025**, *9*, 61.

(18) Lin, Z.; Carvalho, B. R.; Kahn, E.; Lv, R.; Rao, R.; Terrones, H.; Pimenta, M. A.; Terrones, M. Defect engineering of two-dimensional transition metal dichalcogenides. *2D Materials* **2016**, *3*, No. 022002.

(19) Liang, Q.; Zhang, Q.; Zhao, X.; Liu, M.; Wee, A. T. Defect engineering of two-dimensional transition-metal dichalcogenides: applications, challenges, and opportunities. *ACS Nano* **2021**, *15*, 2165−2181.
(20) Xu, X.; Yao, W.; Xiao, D.; Heinz, T. F. Spin and pseudospins in layered transition metal dichalcogenides. *Nat. Phys.* **2014**, *10*, 343−350.
(21) Fang, H.-H.; Wang, X.-J.; Marie, X.; Sun, H.-B. Quantum sensing with optically accessible spin defects in van der Waals layered materials. *Light: Sci. Appl.* **2024**, *13*, 303.
(22) Kohn, W.; Sham, L. J. Self-consistent equations including exchange and correlation effects. *Physical review* **1965**, *140*, A1133.
(23) Soler, J. M.; Artacho, E.; Gale, J. D.; García, A.; Junquera, J.; Ordejón, P.; Sánchez-Portal, D. The SIESTA method for ab initio order-Nmaterials simulation. *J. Phys.: Condens. Matter* **2002**, *14*, 2745.
(24) García, A.; Papior, N.; Akhtar, A.; Artacho, E.; Blum, V.; Bosoni, E.; Brandimarte, P.; Brandbyge, M.; Cerdá, J. I.; Corsetti, F.; et al. Siesta: Recent developments and applications. *J. Chem. Phys.* **2020**, *152*, 204108.
(25) Perdew, J. P.; Burke, K.; Ernzerhof, M. Generalized gradient approximation made simple. *Physical review letters* **1996**, *77*, 3865.
(26) Shafqat, A.; Iqbal, T.; Majid, A. A DFT study of intrinsic point defects in monolayer MoSe2. *AIP Adv.* **2017**, *7*, 105306.
(27) Zhang, H.; Fan, X.-L.; Yang, Y.; Xiao, P. Strain engineering the magnetic states of vacancy-doped monolayer MoSe2. *J. Alloys Compd.* **2015**, *635*, 307−313.
(28) Monkhorst, H. J.; Pack, J. D. Special points for Brillouin-zone integrations. *Phys. Rev. B* **1976**, *13*, 5188.
(29) Humphrey, W.; Dalke, A.; Schulten, K. VMD: visual molecular dynamics. *J. Mol. Graphics* **1996**, *14*, 33−38.
(30) Anisha; Kumar, R.; Srivastava, S. Band gap engineering of 2H-MX2 (M = Mo; X = S, Se, Te) monolayers using strain effect. *Materials Today: Proceedings* **2022**, *54*, 677−681.
(31) Tonndorf, P.; Schmidt, R.; Böttger, P.; Zhang, X.; Börner, J.; Liebig, A.; Albrecht, M.; Kloc, C.; Gordan, O.; Zahn, D. R. T.; et al. Photoluminescence emission and Raman response of monolayer $MoS_2$, $MoSe_2$, and $WSe_2$. *Opt. Express* **2013**, *21*, 4908.
(32) Mak, K. F.; Lee, C.; Hone, J.; Shan, J.; Heinz, T. F. Atomically thin MoS 2: a new direct-gap semiconductor. *Physical review letters* **2010**, *105*, No. 136805.
(33) Yue, Q.; Shao, Z.; Chang, S.; Li, J. Adsorption of gas molecules on monolayer MoS2 and effect of applied electric field. *Nanoscale Res. Lett.* **2013**, *8*, 425.
(34) Li, H.; Huang, M.; Cao, G. Markedly different adsorption behaviors of gas molecules on defective monolayer MoS 2: A first-principles study. *Phys. Chem. Chem. Phys.* **2016**, *18*, 15110−15117.





https://doi.org/10.1021/acsomega.5c10979
*ACS Omega* 2026, 11, 6191−6197